The International Journal of Advanced Manufacturing Technology (2019) 101:2947–2954
https://doi.org/10.1007/s00170-018-3101-8

ORIGINAL ARTICLE

Laser micro-structuring of a coarse-grained diamond grinding wheel

Hui Deng[1] · Zhou Xu[2] · Linqing Wang[2] · Pengcheng Zhu[2]

Received: 26 July 2018 / Accepted: 20 November 2018 / Published online: 13 December 2018

Abstract
To address the significant subsurface damage of a workpiece after grinding by a coarse-grained wheel, the research on nanosecond ultraviolet laser micro-structuring of a coarse-grained diamond-grinding wheel was carried out, and the influence of process parameters on the depth and width of the groove, the micro-structuring efficiency, and the qualification rate of micro-structured grains were explored. The results show that the single-pass laser circular cutting method cannot achieve the desired groove size even with an arbitrarily large number of scanning cycles. The multi-pass laser circular cutting method can effectively improve the micro-structuring efficiency, and the width and depth of the groove increased and decreased respectively with the increase of the pass spacing. The qualification rate of micro-structured grains was related to the groove spacing, the distribution of the grains on the surface of the grinding wheel, the grain diameter, and the groove width. Under the assumption that the grains were evenly distributed on the surface of the grinding wheel, the qualification rate first increased and then decreased with the increase of the groove spacing.

Keywords Diamond grinding wheel · Laser structuring · Structuring efficiency · Qualification rate of grains

1 Introduction

Fine-grained or micro-powder diamond wheels are common tools for precision and ultra-precision grinding of hard and brittle material parts [1, 2]. However, this type of grinding wheel has some drawbacks: A small chip space and a low-retaining strength of the bond cause the surface of the grinding wheel to be easily clogged and the grains to fall off easily, which leads to frequent and time-consuming dressing of the grinding wheel during processing [3, 4].

In view of the advantages of a coarse-grained grinding wheel with a large chip space and a strong bond-holding force, some scholars have tried to use coarse-grained diamond wheel for precision and ultra-precision machining of hard and brittle materials, and found that the surface roughness of the workpiece after grinding can reach the nanometer level [4–6]. However, it was also found that the subsurface damage depth (SSD) of the grinded workpiece increases with the increase of the grain size [7, 8]. The reasons for this are described as follows: After dressing, the top of the grain (Fig. 1a) is cut into a facet (Fig. 1b), which increases the contact area between the grain and workpiece during grinding [9]. Therefore, the cooling liquid cannot easily reach the grinding area. As a result, the normal grinding force and the grinding temperature increases, which eventually leads to an increase in SSD of the workpiece after grinding [10, 11].

To solve this problem, a nanosecond ultraviolet laser beam will be used to cut micron-sized grooves on the surfaces of grains (i.e., laser structuring wheel), as shown in Fig. 1c. This process sought to reduce the contact area of the grain-workpiece and to increase the number of effective cutting edges on the wheel surface. The goal is to improve the surface quality of the workpiece after grinding.

Laser structuring is one of the methods for preparing a structured grinding wheel [12]. A laser beam is used to produce a regularly arranged grooves [13] or blind holes [14] on the surface of the grinding wheel, as shown in Fig. 2. Depending on the dimensions of the groove width (or hole diameter), Li et al. [15] subdivided the structuring into macro-structuring (> 100 μm) and micro-structuring (< 100 μm). Zhang et al. [16] used a laser beam to machine grooves with a width of 1.2 mm, a spacing of 3.5 mm, a depth of 0.85 mm,

✉ Hui Deng
denghnu@163.com

[1] Hunan Provincial Key Laboratory of High Efficiency and Precision Machining of Difficult-to-Cut Material, Hunan University of Science and Technology, Xiangtan 411201, China

[2] School of Mechanical Engineering, Hunan University of Science and Technology, Xiangtan 411201, China

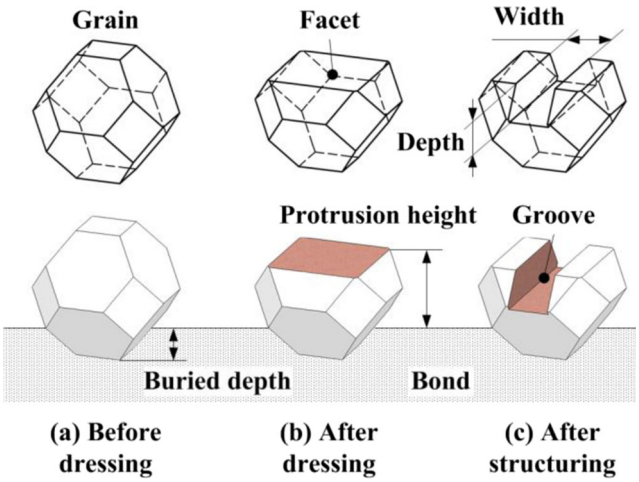

Fig. 1 Schematic diagram of geometric shape of a single grain

and angles of 0°, 30°, 45°, and 90° (the angle between the groove direction and the axis of the grinding wheel) on the surface of a resin-bonded diamond wheel (grain diameter, 120 μm). It was found that compared with a non-structured grinding wheel, the macro-structured grinding wheel can effectively reduce the grinding force, but fails to improve the surface roughness of the grinded workpiece, and the edge of the groove wears faster. A laser beam was used by Guo et al. [17] to produce linear grooves with a width of 10–15 μm, a spacing of 30, 70, 90, and 150 μm, and an angle of 90° on the surface of a single-layer electroplated diamond wheel (grain diameter, 120 μm). It was found that the micro-structured wheel can reduce the SSD of a grinded optical glass by 2–3 μm compared with a non-structured wheel, and the SSD decreases with decreasing groove spacing. In addition, the author also pointed out that because the groove direction of the structured grinding wheel is perpendicular to the axis of the grinding wheel, the cross-sectional shape of the groove is easily reproduced to the surface of the optical glass during grinding, resulting in a large surface roughness of the grinded workpiece, and the surface roughness increases with increasing groove spacing.

In view of this, the nanosecond laser micro-structuring of the coarse-grained diamond grinding wheel will be studied in this paper. First, the effect of a single-pulse energy, number of scanning cycles, the number of scanning passes and pass spacing on the width and depth of the groove, and micro-structuring efficiency will be explored. Then, the effect of groove spacing on the qualification rate of the micro-structured grains will be investigated. Finally, two different patterns of micro-structured diamond grinding wheels will be prepared.

2 Experimental conditions

Figure 3 shows the galvanometer-based laser micro-structuring experimental apparatus. The single-pulse energy e_p was 0.15–0.25 mJ, the pulse frequency f was 30 kHz, the wavelength λ was 355 nm, and the pulse width τ was 18 ns. After the laser beam was reflected by the galvanometer and focused by the lens in the scanning head, it was incident along the normal direction on the surface of the grinding wheel installed at main axis of the surface grinder with a defocusing amount (Δ) of 0 mm and a focal spot diameter (d_f) of 35 μm. The bronze-bonded diamond grinding wheel had a diameter D = 150 mm, a width W = 10 mm, and a grain diameter d = 250 μm. By coordinating the deflection angles of the two galvanometers in the scanning head, the laser beam can be controlled to scan on the surface of the grinding wheel according to any predetermined planar path to prepare various patterns of micro-structured grinding wheels.

Since the surface of the grinding wheel is a cylindrical surface, thereby causing a change in the defocusing amount and the laser power density when laser structuring, so that the dimensional uniformity of the groove after structuring is poor. To this end, the wheel's central angle was equally divided by the angle θ. The geometric relation between the defocusing amount Δ and the angle θ is shown in Fig. 4. When angle θ is small enough, the amount of change in the defocusing amount is small, and its influence on the structuring process is almost negligible. When the arc surface corresponding to an angle θ ($\approx 10°$) was completed, the wheel was rotated by θ along a fixed direction for continued processing until the micro-structuring of the entire wheel surface was completed. Precise control of the rotation angle of the grinding wheel can be realized through the spindle of the grinder with a precision of up to 0.1°.

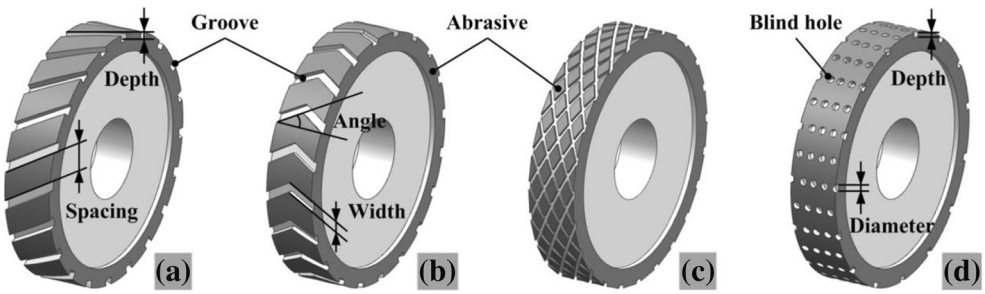

Fig. 2 Laser-structured grinding wheel with different patterns

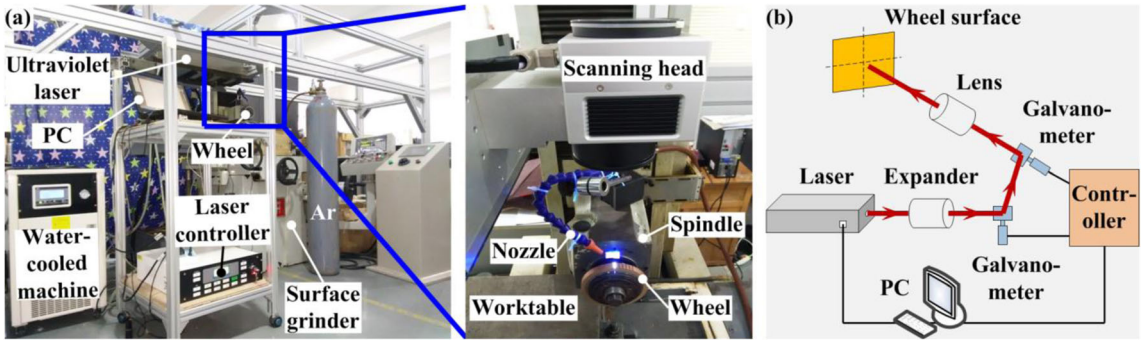

Fig. 3 Experimental apparatus for laser micro-structuring

The three-dimensional microscope with a super depth of field and the video microscopy were used to observe the surface topography of the grinding wheel.

3 Results and discussion

3.1 Groove size

The essence of a laser micro-structuring of grinding wheel is to produce grooves of width w and depth h matching the grain size on the surface of grains, thereby improving grinding performance without affecting the service life of the wheel. If w or h is too large, as shown in Fig. 5a–c, it will lead to a decrease of grain strength or even the loss of cutting edges, aggravating the grain wear and shortening the service life of the wheel. If w or h is too small, as shown in Fig. 5d–e, since the contact area between the grain and workpiece is not reduced sufficiently, the force and heat are not reduced continuously during the grinding process, and therefore, the purpose of improving the grinding performance of the wheel is not achieved. When w and h are about 1/3 and 1/6 of the grain diameter, respectively (Fig. 5f), it can not only ensure the service life of the grain but also improve the cutting performance of the grain. As the grain diameter d was 250 μm for this paper, the appropriate width w and depth h of the groove were approximately 80 and 40 μm, respectively.

3.2 Single-pass laser circular-cutting experiment

Before the laser micro-structuring experiment, the laser cutting experiments of the grinding wheel without protective gas were carried out. Figure 6a shows the three-dimensional surface topography of the grinding wheel after cutting. It can be observed that the color of the interior and the surrounding area of the groove blackens, which is caused by the oxidation of the bronze bond and the oxidation and graphitizing of the diamond. The cross-section of the groove is approximately V-shaped for the following reasons: (1) The laser beam energy in this experiment has a Gaussian distribution, leading to a high material-removal rate in the spot central area of high-energy density and a low material-removal rate in the edge region of low-energy density; (2) with increasing groove depth, the laser-cutting efficiency decreases gradually. The widths of the grooves on the surface of the grains and the bond are basically the same, but the groove depths on the two surfaces are not. This is due to the difference in physical properties of bronze and diamond, and their difference in absorption and transmission of ultraviolet laser energy. Only the size of the groove on the grain's surface was measured. The width of the top of the

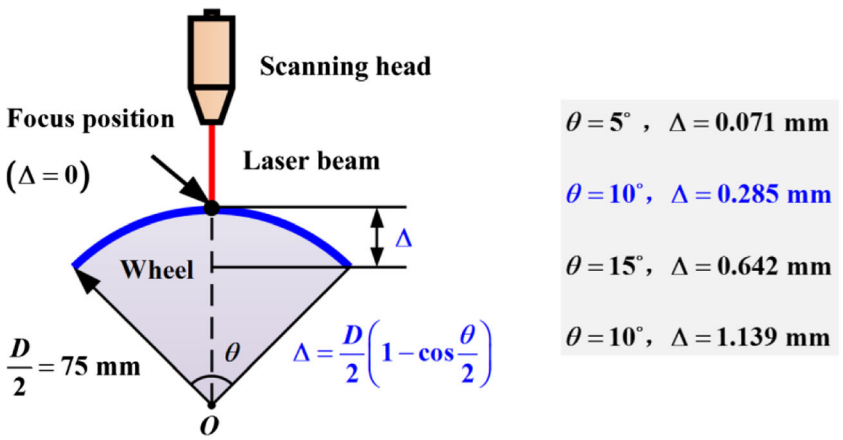

Fig. 4 Geometric relation between the defocusing amount Δ and the angle θ

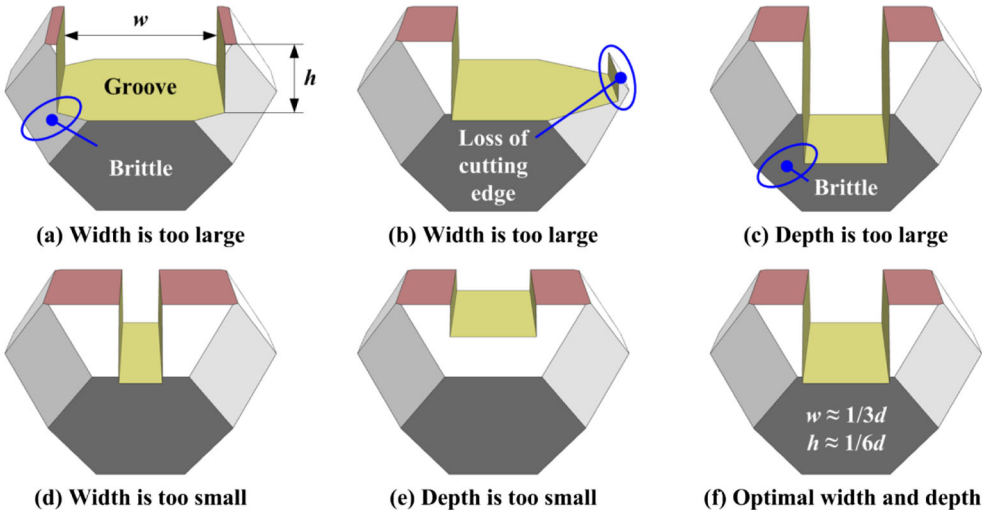

Fig. 5 Schematic diagram of grooves with different sizes

groove was used as the groove width w, and the distance between the bottom of the groove and the surface of the unprocessed grinding wheel was taken as the groove height h.

The laser beam with different single-pulse energy e_p was used to scan circularly 300 times at a speed $v = 800$ mm/s along a single track line parallel to the axis of the wheel (i.e., single-pass laser circular cutting). The groove topography was observed with a 3D optical microscope with an ultra-deep depth of field. The results are shown in Fig. 6b–e. To ensure that the initial conditions were as consistent as possible, four sets of experiments were conducted on the same surface of the bronze-bonded diamond-grinding wheel after laser profiling. It can be observed that when e_p is small (0.15 mJ, 0.18 mJ), h is only approximately 3 μm; when e_p increases to 0.217 mJ, h increases to 8.4 μm; when e_p reaches the maximum single-pulse energy of 0.25 mJ, h grows to 10.5 μm with a speed decrease, and this value is significantly different from the desired value (40 μm).

To this end, the number of scanning cycles in Fig. 6e was increased N from 300 to 1000 times (other parameters were unchanged) and then the experiment was performed. It was found that when N is greater than 600, the plasma, sputtering, and acoustic emission phenomena in the ablation process almost disappear (indicating that the material-removal efficiency was very low). After the experiment, w and h were measured to be only 45.7 and 18.4 μm, respectively (the limit value of the groove size under the current conditions), as shown in Fig. 6f. The reasons are as follows: in the case where the groove width is basically the same, as the groove depth increases, the spatter generated during laser cutting is more difficult to fly away from the processing area; therefore, the amount of the recondensate absorbed on both sides of the groove and accumulated at the bottom of the groove increases, making it increasingly difficult for the laser beam to reach directly to the bottom of the groove. As a result, the efficiency of laser cutting to remove the material gradually decreases until the material cannot be removed at the end, and a limiting groove depth is reached.

In summary, under the present experimental conditions, the single-pass laser circular-cutting method cannot achieve the desired groove size even with an arbitrarily large number of scanning cycles.

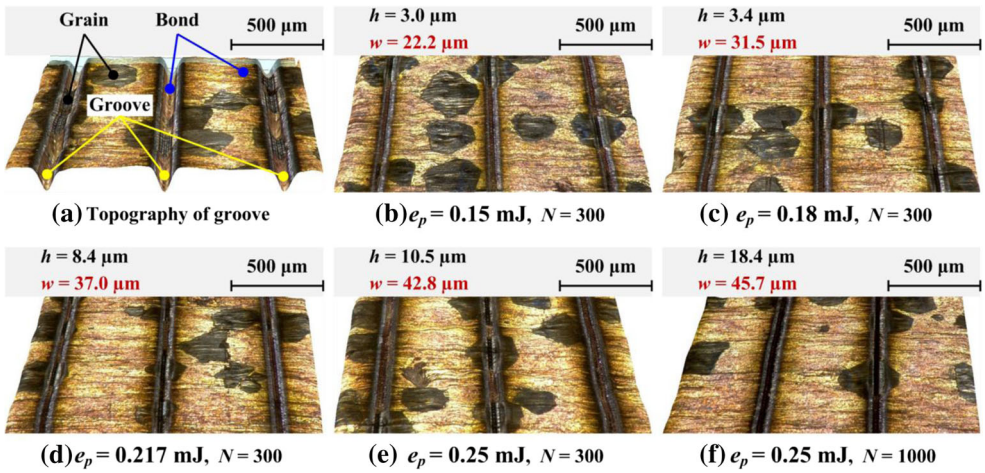

Fig. 6 Topography of the single-pass laser circular-cutting groove

3.3 Multi-pass laser circular-cutting experiment

To solve the problem of the single-pass laser circular cutting method, a multi-pass laser circular-cutting method is proposed in this paper, which is to use a laser beam along the multiple track lines parallel to the axis of the wheel with a center distance of l ($k = 2, 3 \ldots, n$) to cut circularly the wheel surface, as shown in Fig. 7a.

In this section, six sets of multi-pass laser circular-cutting experiments were conducted under the conditions of $e_p =$ 0.25 mJ and $v = 800$ mm/s. The scheme and parameters are shown in Fig. 7. To ensure the same cutting time of each experiment, the number of scanning cycles N was set to 150 for the three sets of experiments with the number of scanning passes $k = 2$. N was set to 100 for the three sets of experiments with $k = 3$. After the experiment, the surface topography of the grinding wheel and the groove size were measured by means of a 3D optical microscopy with an ultra-deep depth of field, as shown in Fig. 8.

In Fig. 8a, the internal color of the groove is darker, the groove width w is measured to be 45.4 μm, and the depth h is 7.4 μm. It can be seen that the groove was still too narrow, and it was difficult for the laser beam to directly reach the bottom of the groove to efficiently remove material. As a result, a large amount of laser energy was absorbed by recondensate in the groove and transmitted to the surrounding area, which exacerbated the oxidation of the bond and oxidation and graphitization of grain in and around the groove. When the pass spacing l is increased to 16 μm, as shown in Fig. 8b, the internal color of the groove is lighter (indicating a decrease in the degree of oxidation and graphitization). The measured w is 50.2 μm and h is 29.2 μm (h is nearly four times than that in Fig. 8a). It can be seen that the efficiency of laser-induced material removal significantly improved when the groove width exceeded 50 μm. When l is increased to 24 μm, as shown in Fig. 8c, the groove internal color is brighter, the measured w is 54.0 μm, and h reduces to 20.4 μm compared with that in Fig. 8b. This occurs because when the groove width exceeds a critical value, the material-removal efficiency of the laser is basically constant, so the total amount of material removed is basically the same during the same period of time; when l is increased from 16 to 24 μm, which inevitably leads to an increase of the groove width and a decrease of the groove depth. When the number of scanning passes $k = 3$, Fig. 8d–f and Fig. 8b–c show similar variation patterns: with the increase of the pass spacing, the inner color of the groove brightens, and the width and depth of the groove increase and decrease, respectively.

In the above experiments, when $k = 3$ and $l = 24$ μm, w and h are 71 and 30 μm, which is the closest to the desired values (80 and 40 μm, respectively) of groove width and depth. To this end, N was increased by increments of 20 from 100 to 200 times in Fig. 8f and then five groups of the experiments (the remaining parameters were unchanged) were conducted. It was found that with the increase of N, w basically remained unchanged and h showed a slow growth trend. When N reaches 140, the two values are 75.3 and 38.2 μm, which are the closest to the desired values of groove width and depth.

3.4 Laser micro-structuring experiment

3.4.1 Groove spacing

The micro-structured grain is qualified when there is one and only one groove on the surface of the grain. The qualification rate of micro-structured grains refers to the percentage of the number of qualified grains to the total number of grains on the surface of the grinding wheel. The greater the qualification rate, the better the structuring effect. The distribution (number and location) of the grooves on the surface of the grains is determined by the groove spacing s. If s is too large, the number of structured grains is too small to meet the requirements; if s is too small, then the number of grooves on the surface of the grains is too large (≥ 2), resulting in a decrease in the strength of the grains and a shortened service life of the grinding wheel, which also does not meet the requirements.

When $s = d–2w = 99.4$ μm, the micro-structuring experiments on the surface of the laser-dressed bronze-bonded diamond-grinding wheel with optimized the process parameters were carried out, and experimental results obtained by video microscopy are shown in the left panel of Fig. 9a. Depending on the distribution of grooves on the grain surface, the micro-structured grains can be classified into three categories, as shown in the right panel of Fig. 9a. In the figure, the gray stripes represent grooves, yellow stripes represent the unstructured surface of the wheel, and the blue ovals (A–D) represent the grain. The grains that their left edge is located between the dashed line 1 (through the left edge of the grain A and parallel to the axis of the wheel) and the dashed line 2 (through the left edge of the

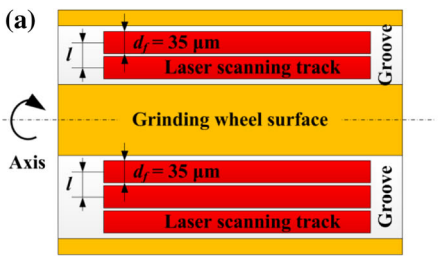

(b)

Number	k	l	N
I	2	8 μm	150
II	2	16 μm	150
III	2	24 μm	150
IV	3	8 μm	100
V	3	16 μm	100
VI	3	24 μm	100

Fig. 7 Experimental scheme and parameters

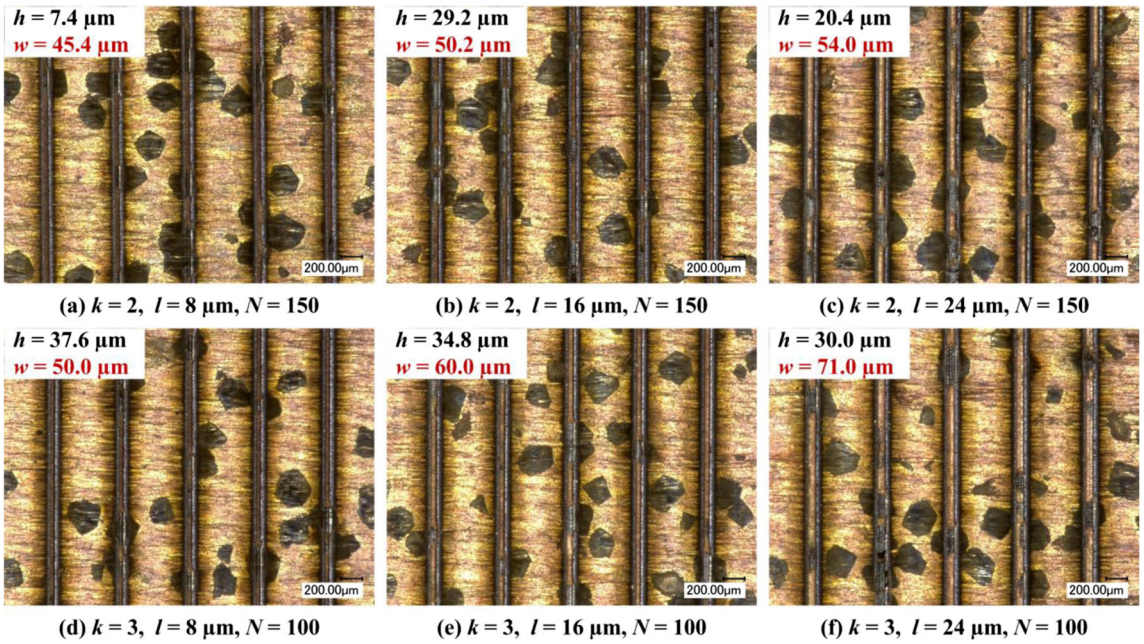

Fig. 8 Topography of the multi-pass laser circular cutting groove

grain B and parallel to the axis of the wheel) (referred to as grains between A and B) have two grooves, and these are unqualified grains. Grains between B and C have one groove, and these are qualified. Grains between C and D have two grooves, and these are unqualified grains.

It can be seen from the above analysis that the qualification rate of grains was related to the groove spacing *s*, the distribution of the grains on the surface of the grinding wheel, the grain diameter *d*, and the groove width *w*, wherein the latter two parameters were constant values in this section. In order to quantify

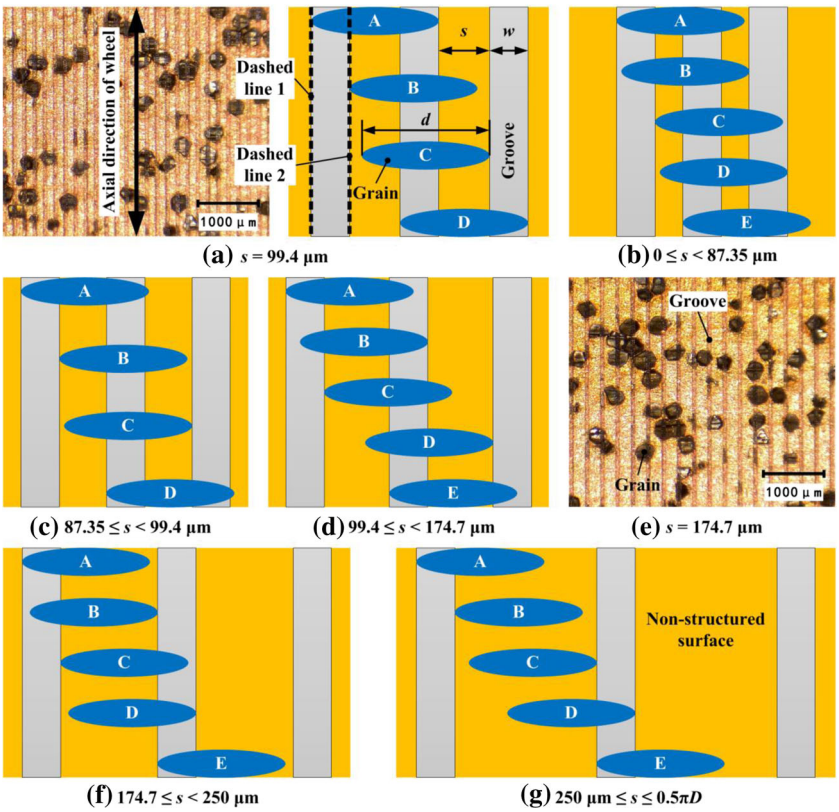

Fig. 9 Distribution of grooves on the grain surface

Fig. 10 Qualification rate of micro-structured grains

(a)

$$\begin{cases} 0 & 0 \le s < 87.35\ \mu m \\ \dfrac{2s+w-d}{w+s} & 87.35 \le s < 99.4\ \mu m \\ & 99.4 \le s < 174.7\ \mu m \\ \dfrac{d-w}{w+s} & 174.7 \le s < 250\ \mu m \\ & 250 \le s \le 157080\ \mu m \end{cases}$$

(c)

Number	Region	Qualified rate
9(b)	None	$\eta = 0$
9(c)	B – C	$0 \le \eta < 12.9\%$
9(d)	C – D	$12.9\% \le \eta < 69.7\%$
9(f)	D – E	$54.6\% < \eta \le 69.7\%$
9(g)	D – E	$0 < \eta \le 54.6\%$

(b)

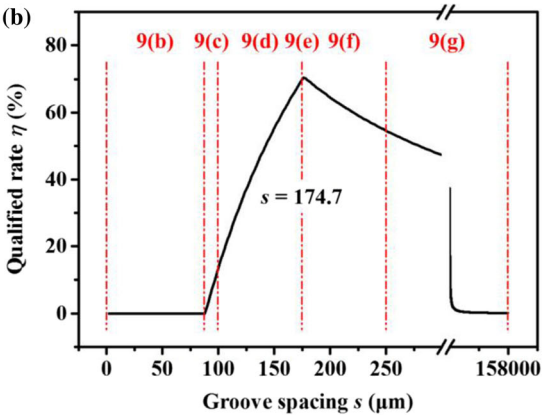

the qualification rate of grains, it was assumed that the grains were uniformly spread over the entire surface of the grinding wheel (in fact, the distribution of the grains on the surface of the grinding wheel is random). At this time, the qualification rate was only related to the groove spacing. Based on this, the qualification rate of micro-structured grains in Fig. 9a was calculated as $\eta = (2\ s + w - d) / (w + s) \times 100\% = 12.9\%$.

Next, the groove spacing $s \in [0, 0.5\pi D]$ was divided into five intervals ($0 \le s < (d - w) / 2$, $(d - w) / 2 \le s < d - 2w$, $d - 2w \le s < d - w$, $d - w \le s < d$, and $d \le s \le 0.5\pi D$), the grains were classified in each interval (Fig. 9b–g), and the qualification rate η of micro-structured grains was calculated, and the results are shown in Fig. 10. When $s \in [0, 87.35\ \mu m)$, there are at least two grooves in each grain, and $\eta = 0$. When $s \in [87.35, 99.4\ \mu m)$, grains between A and B have a groove at the edge; the grain-cutting edge does not increase, and some abrasive is lost, which are unqualified grains. The grains between B and C have single grooves, and they are qualified grains; grains between C and D have two grooves and are unqualified grains; hence, $\eta \in [0, 12.9\%)$. Similarly, when $s \in [99.4, 174.7\ \mu m)$, the grains between C and D are qualified, $\eta \in [12.9, 69.7\%)$; when $s \in [174.7, 250\ \mu m)$, grains between D and E are qualified, $\eta \in (54.6, 69.7\%]$; when $s \in [250, 157{,}080\ \mu m)$, grains between B and C have no groove, and grains between D and E are qualified, $\eta \in (0, 54.6\%]$. In summary, when s increased in the range of $[0, 0.5\pi D]$, the qualification rate η first increased and then decreased, as shown in Fig. 10b. When s was 174.7 μm, η reached its maximum value of 69.7%. Using $s = 174.7\ \mu m$, the surface topography of the micro-structured grinding wheel is shown in Fig. 9e.

3.4.2 Preparation of a micro-structured grinding wheel

Finally, under the conditions of $e_p = 0.25$ mJ, $v = 800$ m/s, $k = 3$, $l = 24\ \mu m$, $N = 140$, $s = 174.7\ \mu m$, and $\alpha = 60°$, the laser micro-structuring experiments with different patterns were performed on the surfaces of two laser-dressed bronze-bonded diamond wheels. Figure 11 shows surface topography of the

Fig. 11 Surface topography of micro-structured grinding wheels with different patterns

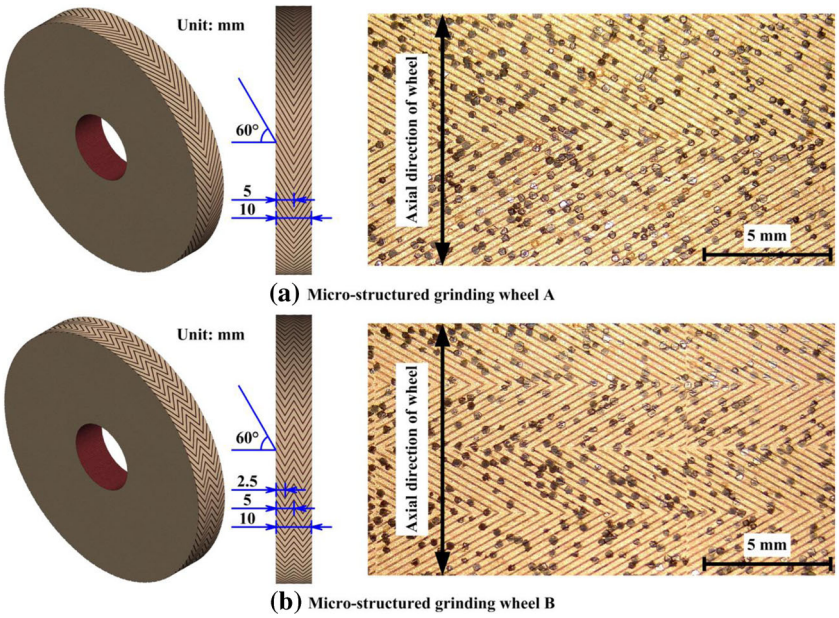

prepared micro-structured grinding wheels A and B. The pattern of wheel A is V-shaped, that of wheel B is W-shaped.

4 Conclusions

In this paper, nanosecond ultraviolet laser cutting and micro-structuring experiments of coarse-grained diamond-grinding wheels were carried out. A new method for the structuring of grinding wheels based on multi-pass laser circular cutting was proposed. The main conclusions are as follows:

(1). Using a $e_p = 0.25$ mJ laser beam single-pass circular cutting the grinding wheel, simply increasing the number of scanning cycles N did not allow the groove width w and depth h to reach the desired value (80 and 40 μm, respectively).

(2). Increasing the number of scanning passes k, i.e., using a multi-pass laser circular-cutting method can effectively improve the efficiency of micro-structuring. By increasing pass spacing l, w increased and h decreased. When $k = 3$, $l = 24$ μm, and $N = 140$, w and h were 75.3 and 38.2 μm, respectively, which were the closest to the desired values.

(3). The qualification rate η of micro-structured grains was related to the groove spacing, the distribution of the grains on the surface of the grinding wheel, the grain diameter, and the groove width. Under the assumption that the grains were uniformly spread over the surface of the grinding wheel, η first increased and then decreased when the groove spacing s was increased in the range of $[0, 0.5\pi D]$. When s was 174.7 μm, η reached a maximum value of 69.7%.

Funding information Financial support for this research was provided by the National Natural Science Foundation of China (No. 51605162) and the Hunan Provincial Natural Science Foundation of China (No. 2017JJ3077).

References

1. Brinksmeier E, Mutluguenes Y, Klocke F, Aurich JC, Shore P, Ohmori H (2010) Ultra-precision grinding. CIRP Ann-Manuf Technol 59:652–671. https://doi.org/10.1016/j.cirp.2010.05.001
2. Stephenson DJ, Sun X, Zervos C (2006) A study on ELID ultra precision grinding of optical glass with acoustic emission. Int J Mach Tool Manu 46:1053–1063. https://doi.org/10.1016/j.ijmachtools.2005.08.013
3. Qian N, Ding W, Zhu Y (2018) Comparative investigation on grindability of K4125 and Inconel718 nickel-based superalloys. Int J Adv Manuf Technol 97:1649–1661. https://doi.org/10.1007/s00170-018-1993-y
4. Zhao Q, Guo B (2015) Ultra-precision grinding of optical glasses using mono-layer nickel electroplated coarse-grained diamond wheels. Part 1: ELID assisted precision conditioning of grinding wheels. Precis Eng 39:56–66. https://doi.org/10.1016/j.precisioneng.2014.07.006
5. Brinksmeier E, Riemer O, Rickens K, Berger D (2016) Application potential of coarse-grained diamond grinding wheels for precision grinding of optical materials. Prod Eng 10:563–573. https://doi.org/10.1007/s11740-016-0699-y
6. Heinzel C, Rickens K, Trumpold H (2009) Engineered wheels for grinding of optical glass. CIRP Ann-Manuf Technnol 58:315–318. https://doi.org/10.1016/j.cirp.2009.03.096
7. Blaineau P, Andre D, Laheurte R, Darnis P, Darbois N, Cahuc O, Neauport J (2015) Subsurface mechanical damage during bound abrasive grinding of fused silica glass. Appl Surf Sci 353:764–773. https://doi.org/10.1016/j.apsusc.2015.07.047
8. Belkhir N, Bouzid D, Lakhedari F, Aliouane T, Raedlein E (2011) Characterization of glass surface damaged by alumina abrasive grains. J Non-Cryst Solids 357:2882–2887. https://doi.org/10.1016/j.jnoncrysol.2011.03.026
9. Mao C, Zhang Y, Peng X, Zhang B, Hu Y, Bi Z (2018) Wear mechanism of single cBN-WC-10Co fiber cutter in machining of Ti-6Al-4V alloy. J Mater Process Technol 259:45–57. https://doi.org/10.1016/j.jmatprotec.2018.04.015
10. Liu C, Ding W, Yu T, Yang C (2018) Materials removal mechanism in high-speed grinding of particulate reinforced titanium matrix composites. Precis Eng 51:68–77. https://doi.org/10.1016/j.precisioneng.2017.07.012
11. Mao C, Lu J, Zhao Z, Yin L, Hu Y, Bi Z (2018) Simulation and experiment of cutting characteristics for single cBN-WC-10Co fiber. Precis Eng 52:170–182. https://doi.org/10.1016/j.precisioneng.2017.12.001
12. Forbrigger C, Bauer R, Warkentin A (2017) A review of state-of-the-art vitrified bond grinding wheel grooving processes. Int J Adv Manuf Technol 90:2207–2216. https://doi.org/10.1007/s00170-016-9546-8
13. Walter C, Komischke T, Kuster F, Wegener K (2014) Laser-structured grinding tools - generation of prototype patterns and performance evaluation. J Mater Process Technol 214:951–961. https://doi.org/10.1016/j.jmatprotec.2013.11.015
14. Rabiey M (2010) Dry grinding with CBN wheels, the effect of structuring. Dissertation, University of Stuttgart
15. Li HN, Axinte D (2016) Textured grinding wheels: a review. Int J Mach Tool Manu 109:8–35. https://doi.org/10.1016/j.ijmachtools.2016.07.001
16. Zhang XH, Kang ZX, Li S, Wu QP, Zhang ZC (2018) Experimental investigations on the impact of different laser macro-structured diamond grinding wheels on alumina ceramic. Int J Adv Manuf Technol 96:1959–1969. https://doi.org/10.1007/s00170-018-1644-3
17. Guo B, Zhao Q, Fang X (2014) Precision grinding of optical glass with laser micro-structured coarse-grained diamond wheels. J Mater Process Technol 214:1045–1051. https://doi.org/10.1016/j.jmatprotec.2013.12.013